Randomized lasso associates freshwater lake-system specific bacterial taxa with heterotrophic production through flow cytometry

Running Title: Linking taxa with production through flow cytometry

Peter Rubbens[1*#], Marian L. Schmidt[23*#], Ruben Props[4], Bopaiah A. Biddanda[5], Nico Boon[4], Willem Waegeman[1], Vincent J. Denef[2]

[*]Peter Rubbens and Marian L. Schmidt contributed equally to this work.

[#]Corresponding author: marschmi@umich.edu, peter.rubbens@ugent.be

[1]KERMIT, Department of Data Analysis and Mathematical Modelling, Ghent University, Coupure Links 653, B-9000, Gent, Belgium;

[2]Department of Ecology and Evolutionary Biology, University of Michigan, 1105 North University Ave., Ann Arbor, MI 48109, USA;

[3]Current address: Department of Integrative Biology, University of Texas at Austin, 2506 Speedway, Austin, Texas 78712, USA;

[4]CMET, Center for Microbial Ecology and Technology, Ghent University, Coupure Links 653, B-9000, Gent, Belgium;

[5]Annis Water Resources Institute, Grand Valley State University, 740 West Shoreline Drive, Muskegon, MI 49441, USA

Abstract

High- (HNA) and low-nucleic acid (LNA) bacteria are two operational groups identified by flow cytometry (FCM) in aquatic systems. HNA cell density often correlates strongly with heterotrophic production, while LNA cell density does not. However, which taxa are specifically associated with these groups, and by extension, productivity has remained elusive. Here, we addressed this knowledge gap by using a machine learning-based variable selection approach that integrated FCM and 16S rRNA gene sequencing data collected from 14 freshwater lakes spanning a broad range in physicochemical conditions. There was a strong association between bacterial heterotrophic production and HNA absolute cell abundances ($R^2 = 0.65$), but not with the more abundant LNA cells. This solidifies findings, mainly from marine systems, that HNA and LNA could be considered separate functional groups, the former contributing a disproportionately large share of carbon cycling. Taxa selected by the models could predict HNA and LNA absolute cell abundances at all taxonomic levels, with the highest performance at the OTU level. Selected OTUs ranged from low to high relative abundance and were mostly lake system-specific (89.5%-99.2%). A subset of selected OTUs was associated with both LNA and HNA groups (12.5%-33.3%) suggesting either phenotypic plasticity or within-OTU genetic and physiological heterogeneity. These findings may lead to the identification of systems-specific putative ecological indicators for heterotrophic productivity. Generally, our approach allows for the association of OTUs with specific functional groups in diverse ecosystems in order to improve our understanding of (microbial) biodiversity-ecosystem functioning relationships.

Importance

A major goal in microbial ecology is to understand how microbial community structure influences ecosystem functioning. Research is limited by the ability to readily culture most bacteria present in the environment and the difference in bacterial physiology *in situ* compared to in laboratory culture. Various methods to directly associate bacterial taxa to functional groups in the environment are being developed. In this study, we applied machine learning methods to relate taxonomic data obtained from marker gene surveys to functional groups identified by flow cytometry. This allowed us to identify the taxa that are associated with heterotrophic productivity in freshwater lakes and indicated that the key contributors were highly system-specific, regularly rare members of the community, and that some could switch between being low and high contributors. Our approach provides a promising framework to identify taxa that contribute to ecosystem functioning and can be further developed to explore microbial contributions beyond heterotrophic production.

Keywords

bacterioplankton, 16S rRNA, flow cytometry, machine learning, variable selection, aquatic microbiology, heterotrophic productivity

Introduction

A key goal in the field of microbial ecology is to understand the relationship between microbial diversity and ecosystem functioning. However, it is challenging to associate bacterial taxa to specific ecosystem processes. Marker gene surveys have shown that natural bacterial communities are extremely diverse and the presence of a taxon does not imply its activity. The taxa observed in these surveys may have low metabolic potential, be dormant, or have recently died (1, 2). An additional hurdle is that the current standard unit of measure for microbial taxonomic analysis is relative abundance. This results in a negative correlation bias (3), which makes it difficult to quantitatively associate specific microbial taxa with microbial ecosystem functions using traditional correlation measures (4). Therefore, in order to ultimately model and predict bacterial communities, new methodologies, which integrate different data types, are needed to associate bacterial taxa with ecosystem functions (5).

One such advance is the use of flow cytometry (FCM), which has been used extensively to study aquatic microbial communities (6–8). This single-cell technology partitions individual microbial cells into phenotypic groups based on their observable optical characteristics. Most commonly, cells are stained with a nucleic acid stain (*e.g.* SYBR Green I) and upon analysis assigned to either a low nucleic acid (LNA) or a high nucleic acid (HNA) group (9–12). HNA cells differ from LNA cells in both a considerable increase in fluorescence due to cellular nucleic acid content and scatter intensity due to cell morphology. The HNA group is thought to contribute more, whereas the LNA population has been considered to contribute less to productivity of a microbial community (6, 13–15). This is based on positive linear relationships between HNA abundance and (a) bacterial heterotrophic production (BP) (10, 14–17), (b) bacterial activity

82 measured using the dye 5-cyano-2,3-ditolyl tetrazolium chloride (18, 19), (c) phytoplankton
83 abundance (20), and (d) dissolved organic carbon concentrations (21). Additionally, growth rates
84 are higher for HNA than LNA cells (13, 16, 22) and HNA cells accrue cell damage significantly
85 faster than the LNA cells under temperature (23) and chemical oxidant stress (24). In contrast,
86 LNA bacterial growth rates are positively correlated with temperature and negatively correlated
87 with chlorophyll a (25). However, it is important to note that LNA cells are often smaller than
88 HNA cells (12, 25–27) and therefore LNA cells could have similar amino acid incorporation
89 rates compared to HNA cells when evaluating biomass-specific production (12).
90
91 Here we used a data-driven approach to associate the dynamics of individual taxa with those of
92 the LNA and HNA groups in freshwater lakes by adopting a machine learning variable selection
93 strategy. We applied two variable selection methods, the Randomized Lasso (RL) (28) and the
94 Boruta algorithm (29) to associate individual taxa with HNA and LNA cell abundances. These
95 methods extend on traditional machine learning algorithms (*i.e.* the Lasso and Random forest
96 algorithm for the RL and Boruta algorithm, respectively) by making use of resampling and
97 randomization. These extensions are needed as (a) the Lasso algorithm is not suited for
98 compositional data because the regression coefficients have an unclear interpretation, and single
99 variables may be selected when correlated to other variables (30), and (b) Random Forest
100 algorithms can be biased towards correlated variables (31), which is an intrinsic issue with
101 relative abundance data (3). The extended methods allow the user to either assign a probability of
102 selection (RL) or statistically decide which taxa to select (Boruta).
103

104 We gathered samples from three types of lake systems (i) a set of oligo- to eutrophic small inland
105 lakes, (ii) a short residence time mesotrophic freshwater estuary lake (Muskegon Lake), and (iii)
106 a large oligotrophic Great Lake (Lake Michigan), all located in Michigan, USA. We then used
107 the RL and Boruta algorithms to associate specific bacterial taxa to HNA and LNA FCM
108 functional groups, and via the observed HNA-productivity relationship, to functioning. To
109 validate the RL-based association with the HNA and/or LNA group, we correlated taxon
110 abundances with specific regions within the FCM fingerprint at finer resolution (*i.e.* bins)
111 without prior knowledge of the HNA/LNA groups. Furthermore, we tested for phylogenetic
112 conservation of HNA and LNA functional groups using the probabilities from the RL output and
113 for the association between the selected taxa and productivity.

Results

Study lakes are dominated by LNA cells

The inland lakes (6.3 x 10^6 cells/mL) and Muskegon Lake (6.0 x 10^6 cell/mL) had significantly higher total cell abundances than Lake Michigan (1.7 x 10^6 cell/mL; p = 2.7 x 10^{-14}). Across all lakes, the mean proportion of HNA cell counts (HNAcc) to total cell counts was much lower (30.4 ± 9%) compared to the mean proportion of LNA cell counts (LNAcc; 69.6 ± 9%). Through ordinary least squares regression, there was a strong correlation between HNAcc and LNAcc across all data (R^2 = 0.45, P = 2 x 10^{-24}; **Figure 1A**), however, only Lake Michigan (R^2 = 0.59, P = 5 x 10^{-11}) and Muskegon Lake (R^2 = 0.44, P= 2 x 10^{-9}) had significant correlations when the three ecosystems were considered separately.

HNA cell counts and heterotrophic bacterial production are strongly correlated

For mesotrophic Muskegon Lake, there was a strong correlation between total bacterial heterotrophic production and HNAcc (R^2 = 0.65, P = 1e-05; **Figure 1B**), no correlation between BP and LNAcc (R^2 = 0.005, P = 0.31; **Figure 1C**), and a weak correlation between heterotrophic production and total cell counts (R^2 = 0.18, P = 0.03; **Figure 1D**). There was a positive (HNA) and negative (LNA) correlation between the fraction of HNA or LNA to total cells and productivity, however, the relationship was weak and not significant (R^2 = 0.14, P = 0.057).

Association of OTUs to HNA and LNA groups by Randomized Lasso

The relevance of specific OTUs for predicting FCM functional group abundance was assessed using the Randomized Lasso (RL), which assigns a score between 0 (unimportant) to 1 (highly important) to each taxon in function of the target variable: HNAcc or LNAcc. To assess the

predictive power of a subset of OTUs based on the RL, we iteratively removed the OTUs with the lowest RL score in a recursive variable elimination scheme. R^2_{CV}, a goodness-of-fit measure using the R^2 of how well a set of selected OTUs predicts HNAcc or LNAcc compared to true values using cross-validation, increased when lower-ranked OTUs were removed (moving from right to left on **Figure 2**). The increase was gradual for the inland lakes (**Figure 2A**) and Muskegon Lake (**Figure 2C**) but was abrupt for Lake Michigan (**Figure 2B**). The proportion of taxa that resulted in the highest R^2_{CV} (*see solid (HNA) and dotted (LNA) lines in* **Figure 2**) was 10.2% of all taxa for HNA and 17.7% for LNA for the inland lakes, 4.0% for HNA and 3.0% for LNA for Lake Michigan, and 21.1% for both HNA and LNA in Muskegon Lake. Lake Michigan differed the most from other lake systems, having the lowest R^2_{CV}, a sharp increase in R^2_{CV} as OTUs were eliminated, and a considerably lower number of OTUs that were retained (13 for HNAcc, 10 for LNAcc). No relationship could be established between rankings of variable selection methods and the relative abundance of individual OTUs (**Figure S1**). HNAcc and LNAcc could be predicted with equivalent performance to relative HNA and LNA proportions, yet the increase between initial and optimal performance was larger (**Figure S2**). The final predictive performance was higher when relative OTU abundances were transformed using the CLR-transformation (**Figure S3**).

OTU-level predictions outperform other taxonomic levels

R^2_{CV} values were considerably higher than zero on all taxonomic levels, indicating that our results were consistent across all taxonomic levels and that different levels can be related to changes in HNAcc and LNAcc. While the OTU level resulted in the best prediction of HNAcc and LNAcc (**Figure 3**), each individual OTU had a lower RL score compared to other taxonomic levels,

which on average became lower as the taxonomic level decreased (**Figure S4**). The fraction of variables (*i.e.* taxa) that could be removed to reach the maximum R^2_{CV} decreased as the taxonomic level became less resolved.

Validation of RL OTU selection results using the Boruta algorithm and Kendall tau statistic

Venn diagrams were constructed to visualize consistency in the number of OTUs that were selected according to the RL method, the Boruta algorithm, and individual correlations with HNAcc and LNAcc via the Kendall rank correlation coefficient (**Figure S5**). The Kendall rank correlation coefficient selected the most OTUs, followed by the RL, and then the Boruta algorithm (except for HNAcc in Lake Muskegon; **Figure S5**). The Boruta algorithm selects relevant variables based on the importance of the most permuted variable as retrieved from multiple Random Forest models (*see materials and methods*). The Boruta algorithm ranks selected OTUs as '1', tentative OTUs as '2', and all other OTUs have lower ranks, depending on the stage in which they were eliminated. The fraction of selected OTUs was always smaller than 1% across lake systems and functional groups (**Figure S6)**. All methods agreed on only a small subset of OTUs.

For each lake system individually, the top RL-scored OTU for HNAcc was also selected by the Boruta algorithm, whereas both methods only agreed for Lake Michigan LNAcc (**Table 1**). Across all lake systems, OTU060 (Proteobacteria;Sphingomonadales;alfIV_unclassified) was the only OTU selected across all lake systems (LNAcc-associated). As Random Forest regressions are the base method of the Boruta algorithm, we compared the predictive power of Boruta selected OTUs to those of all OTUs using Random Forest regression. For all lake systems and

functional groups, the performance increased when only Boruta-selected OTUs were included in the model (**Figure S7)**. Lasso predictions, in which OTUs were selected according to the RL, were better as opposed to Random Forest predictions in which OTUs were selected according to the Boruta algorithm (**Figure S7**).

Although all methods only agreed on a minority of OTUs, we can still formulate a number of general conclusions across these methods: (1) the selected OTUs were mostly lake systems specific, (2) a small fraction of OTUs was needed to predict changes in community composition, (3) selected OTUs were associated with absolute HNA or LNA abundance, (4) top RL-ranked HNA-associated OTUs were also selected according to the Boruta algorithm and (5) when the RL and Boruta both agreed on an OTU it was always significantly correlated with both HNAcc or LNAcc.

HNA- and LNA-associated OTUs differed across lake systems

RL-selected OTUs were mostly assigned to either the HNA or LNA groups and there was limited correspondence across lake systems between the selected OTUs (**Figure 4**). 1.5%-1.9% of the OTUs selected for Lake Michigan were also associated with HNAcc or LNAcc for the inland lakes or Muskegon Lake. This amount was higher for the shared OTUs between the inland lakes and Lake Muskegon, but still only amounted to 6.0% (HNAcc) or 10.5% (LNAcc) of all common OTUs. For OTUs selected in all three freshwater environments, RL scores were lake ecosystem specific, with only a significant similarity between the Inland lakes and Muskegon lake for HNAcc ($r = 0.21$, $P = 0.0042$; **Figure S8**). The Boruta algorithm selected mostly OTUs that were unique both for the lake system and FCM group (**Figure S9**).

206

207 The Bacteroidetes, Betaproteobacteria, Alphaproteobacteria, and Verrucomicrobia contributed
208 54% of the 258 OTUs selected by the RL (**Figure 5**). Most selected OTUs belonging to these
209 four phyla were associated with the LNA group (41-52% of selected OTUs), less than one third
210 with the HNA group (14-30% of selected OTUs), and the remainder were selected as associated
211 with both the LNA and HNA groups (23-36% of selected OTUs). In Muskegon Lake, OTU173
212 (Bacteroidetes;Flavobacteriales;bacII-A) was selected as the major HNA-associated taxon while
213 OTU29 (Bacteroidetes;Cytophagales;bacIII-B) had the highest RL score for LNA OTUs. In Lake
214 Michigan, OTU25 (Bacteroidetes;Cytophagales;bacIII-A), was selected as the major HNA-
215 associated taxon while OTU168 (Alphaproteobacteria:Rhizobiales:alfVII) was selected as a
216 major LNA-associated taxon. For the inland lakes, OTU369
217 (Alphaproteobacterial;Rhodospirillales;alfVIII) was the major HNA-associated OTU while the
218 OTU555 (Deltaproteobacteria;Bdellovibrionaceae;OM27) was the major LNA-associated taxon.
219 Most OTUs were selected for Muskegon Lake (153 OTUs; compared to 136 OTUs from the
220 Inland Lakes and 20 OTUs from Lake Michigan) and 33% of these OTUs were associated with
221 both FCM groups.

222

223 ***Association with HNA and LNA is not phylogenetically conserved***

224 To evaluate how much evolutionary history explains whether a selected taxon was associated
225 with the HNA and/or LNA group(s), we calculated Pagel's λ, Blomberg's K, and Moran's I,
226 which are different measures for testing whether there was a phylogenetic conservation of these
227 traits. No phylogenetic signal was detected when using Pagel's λ with either using FCM
228 functional group as a discrete variable (*i.e.* associating an OTU with HNA, LNA, or Both or in

relation to the HNA RL score, which is a continuous variable (lambda = 0.16; P = 1) (**Figure 5**). However, there was a significant phylogenetic signal for the LNA RL score ($p = 0.003$, $\lambda = 0.66$), suggesting a stronger phylogenetic structure in the LNA group compared to the HNA group. This significant result in the LNA group was not found when other measures of phylogenetic signal were considered (Blomberg's K (HNA: $p = 0.63$; LNA: $p = 0.54$), and Moran's I (HNA: $p = 0.88$; LNA: $p = 0.12$)).

Flow cytometry fingerprints confirm associated taxa and reveal more complex relationships between taxonomy and flow cytometric features

To confirm the association of the final selected OTUs with the HNA and LNA groups, and resolve how HNA and LNA groups correspond to OTU-level clustering of cells on the FCM fingerprints, we calculated the correlation between the density of individual small regions (*i.e.* "bins") in the flow cytometry data with the relative abundances of the OTUs. Note that (i) as these values denote correlations, they do not indicate actual presence, and (ii) the threshold that was used to manually make the distinction between HNAcc and LNAcc (*i.e.* dotted line in **Figure 6**) lies very close to the border between the two regions of positive and negative correlation. OTU25 correlated with bins that when aggregated corresponded to almost the entire HNA region, whereas OTU173 was limited to bins corresponding to the bottom of the HNA region (**Figure 6**). In contrast, OTU369 was positively correlated to bins situated in both the LNA and HNA regions of the cytometric fingerprint, highlighting results from **Figure 4** where OTU369 was selected for both HNA and LNA.

Proteobacteria and rare taxa correlate with productivity measurements

The Kendall rank correlation coefficient was calculated between CLR-transformed abundances of individual OTUs and productivity measurements. OTU481 was the sole OTU that correlated with productivity after a multiple testing correction (Kendall's tau-b = -0.67, P = 0.00003, P_adj = 0.016), but had a low RL score (0.022) for HNAcc and was not selected according to the Boruta algorithm. Of the top 10 OTUs selected for HNAcc according to the RL, three were still significantly associated with productivity (OTU614: P = 0.0064; OTU412, P = 0.044; OTU487, P = 0.014), but not when corrected for multiple hypothesis testing. Some OTUs that had a high RL score also had a positive response to productivity measurements, though they were insignificant after multiple testing correction. At the phylum level, only Proteobacteria were significantly correlated to productivity measurements (Kendall's tau = 0.49, P = 0.002, P_adj = 0.05).

Discussion

Our study furthers the integration of functional and genotypic information to determine the complex relationships between microbial diversity and ecosystem functioning. Our results confirmed previous findings that flow cytometric operational groups are distinct functional groups having divergent correlations with heterotrophic productivity. Using two machine learning based variable selection strategies, we could associate bacterial taxa identified by 16S rRNA gene sequencing to these two functional groups in three types of freshwater lake systems in the Great Lakes region. We revealed that (i) HNA and LNA cell abundances were best predicted by a small subset of OTUs that were unique to each lake type, (ii) some OTUs were included in the best model for both HNA and LNA abundance, (iii) there was no phylogenetic conservation of HNA and LNA group association and (iv) freshwater FCM fingerprints display

more complex patterns related to OTUs and productivity compared to the traditional dichotomy of HNA and LNA.

Although high-nucleic acid cell counts (HNAcc) and low-nucleic acid cell counts (LNAcc) were correlated with each other, only the association between bacterial heterotrophic production (BP) and HNAcc was strong and significant. This is in line with previous reports, though past studies have focused on the proportion of HNA rather than absolute cell abundances and are strongly biased towards marine systems. For example, Bouvier et al. (11) found a correlation between the fraction of HNA cells and BP within a large dataset of 640 samples across various freshwater to marine environments (Pearson's r = 0.49), whereas a study off the coast of the Antarctic Peninsula found a moderate correlation (R^2 = 0.36; (17)). Another study in the Bay of Biscay also found this association (R^2 = 0.16; (15)), however, the authors attributed this difference to be related to cell size and not due to the activity of HNA. Notably, these studies were predominantly testing the association of marine HNA groups. The high correlation coefficients observed in our study may indicate a strong coupling between freshwater carbon cycling and HNA group abundance in freshwater lake systems. Consequently, this suggests an important role of HNA bacteria in the disproportionately large role that freshwater systems in the global carbon cycle (32). It has to be noted that our study only evaluated bacterial heterotrophic production using leucine amino acid incorporation, which biases our analyses against bacterial groups that cannot import or assimilate this compound (33). Finally, as our correlations with proportional HNA group abundances also indicated less strong correlations than with absolute HNAcc, we suggest absolute HNAcc should be used to best predict and study heterotrophic bacterial production.

298 Similar to other microbiome studies that use machine learning, only a minority of OTUs were
299 needed to predict the phenotype of interest, with low predictive power of each single OTU, but
300 strong predictive capacity of the selected group of OTUs (17, 34–36). Both the RL and Boruta
301 algorithm have been applied to microbiome studies before, for example in the selection of genera
302 in the human microbiome associated with BMI (37), salivary pH and lysozyme activity (38), and
303 in relation to multiple sclerosis (39) or with differing diets during primate pregnancy (40). The
304 Boruta algorithm has also recently been proposed as one of the top-performing variable selection
305 methods that make use of Random Forests (41). Despite the power of these approaches,
306 improvements can be made when attempting to integrate different types of data. For example,
307 16S rRNA gene sequencing still faces the hurdles of DNA extraction (42) and 16S copy number
308 bias (43). Moreover, detection limits are different for FCM (expressed in the number of cells)
309 and 16S rRNA gene sequencing (expressed in the number of gene counts or relative abundance),
310 therefore creating data that may be different in resolution.
311
312 The selection of different sets of HNA and LNA OTUs across the three freshwater systems
313 indicates that different taxa underlie the universally observed HNA and LNA functional groups
314 across aquatic systems. This is perhaps not surprising as it has been shown that there is strong
315 species sorting in lake systems (44, 45), shaping community composition through diverging
316 environmental conditions between the lake systems presented here (46). This high system
317 specificity also explains the low RL scores for individual OTUs, as the spatial and temporal
318 dynamics of an OTU diverged strongly across systems. For example, an OTU that has an RL
319 score of 0.5 implies that on average it will only be chosen one out of two times in a Lasso model.
320

Some OTUs were associated with both HNAcc and LNAcc. There are multiple possible explanations for this: (a) In line with scenario 1 from Bouvier et al (11), cells transition from active growth (primarily HNA) to death or a dormant state (primarily LNA), depending on variable conditions over the spatiotemporal gradients sampled in this study. A large fraction of cells (40-95%) in aquatic systems has indeed been inferred to be dormant (47–49), in line with the predominance of LNA cells. (b) The same OTU may occur in both HNA and LNA groups due to phenotypic plasticity, which is more in line with scenario 4 from Bouvier et al (11). Bacterial phenotypic plasticity in size and morphology has been observed (50), and agrees with suggestions that HNA and LNA groups correspond to cells of differing size (12, 15, 27). (c) The association of taxa to LNA and HNA can also mean that these taxonomic groups thrive within either high or low productivity ecosystems and not necessarily that they are responsible for the change in productivity. (d) Finally, OTU level grouping of bacterial taxa can disguise genomic and corresponding phenotypic heterogeneity (51–54), which may be an alternate explanation for inconsistent associations between OTUs and FCM functional groups.

We found no clear phylogenetic conservation of association to HNAcc or LNAcc. This is in contrast to a recent study that found a clear signal at the phylum level across different aquatic systems (27). However, lake water samples were an exception to the general trend. In addition, it is notable that Proctor et al. (27) separated HNA and LNA cells based on cell size (where HNA cells were defined at approximately >0.4 **μ**m and LNA cells were approximately 0.2-0.4 **μ**m, based on 50-90% removal of HNA cells after filtering using a 0.4 **μ**m filter), while our study separated these FCM functional groups on the basis of fluorescence intensity alone. A more direct estimation of phylogenetic conservation that directly combines cell sorting of HNA or

LNA cells and sequencing, such as the approach of Vila-Costa et al. (55), will be needed to resolve these contrasting results. Considering the correlations between FCM-based phenotypic diversity and sequencing-based taxonomic diversity (56, 57), there clearly is a link between taxonomy and the structure in microbial cytometry data (17). However, the HNA/LNA dichotomy is too unresolved, as our correlation analysis between smaller regions in the cytometric fingerprint and the highly-ranked OTUs revealed a more complex relationship. This agrees with recent research, in which more than two FCM operational groups in aquatic systems were identified (17, 58, 59)7).

The Boruta algorithm and RL scores agreed on a small subset of OTUs, including the top-ranked HNA OTU for all lake systems according to RL, which motivates further investigation of the ecology of these OTUs. While little detailed information on the identities and ecology of HNA and LNA freshwater lake bacterial taxa exists, several studies identified Bacteroidetes among the most prominent HNA taxa, which is in line with our findings. Independent research by Vila-Costa et al. (55) found that the HNA group was dominated by Bacteroidetes in summer samples from the Mediterranean Sea, Read et al. (19) showed that HNA abundances correlated with Bacteroidetes, and Schattenhofer et al. (60) reported that the Bacteroidetes accounted for the majority of HNA cells in the North Atlantic Ocean. In Muskegon Lake, OTU173 was the dominant HNA taxon and is a member of the Order *Flavobacteriales* (bacII-A). The bacII group is a very abundant freshwater bacterial group and has been associated with senescence and decline of an intense algal bloom (61), suggesting their potential for bacterial production. BacII-A has also made up ~10% of the total microbial community during cyanobacterial blooms, reaching its maximum density immediately following the bloom (62). In Lake Michigan,

OTU25, a member of the Bacteroidetes Order *Cytophagales* known as bacIII-A, was the top HNA OTU. However, much less is known about this specific group of Bacteroidetes. Though, the bacII-A/bacIII-A group has been strongly associated with more heterotrophically productive headwater sites (compared to higher order streams) from the River Thames, showing a negative correlation in rivers with dendritic distance from the headwaters, indicating that these taxa may contribute more to productivity (19). In the inland lakes, OTU369 was the major HNA taxon and is associated with the Alphaproteobacteria Order Rhodospirillales (alfVIII), which to our knowledge is a group with very little information available in the literature. In contrast to our findings of Bacteroidetes and Alphaproteobacterial HNA selected OTUs, Tada & Suzuki (63) found that the major HNA taxon from an oceanic algal culture was from the Betaproteobacteria whereas LNA OTUs were within the Actinobacteria phylum.

Conclusions

We integrated flow cytometry (FCM) and 16S rRNA gene amplicon sequencing data to associate bacterial taxa with productivity in freshwater lake systems. Our results on a diverse set of freshwater lake systems indicate that the taxa associated with HNA and LNA functional groups are lake-specific, and that association with these functional groups is not phylogenetically conserved. With this study, we show the potential and limitations of integrating flow cytometry-derived *in situ* functional information with sequencing data using machine learning approaches. This integration of data enhances our insights into which taxa may contribute to ecosystem functioning in aquatic bacterial communities. While these data-driven hypotheses will need further verification, the method is promising considering the wide application of FCM in aquatic environments, its recent application in other sample matrices (*e.g.*, faeces (64), soils (65), and

389 wastewater sludge (66)), and the introduction of novel stains to delineate operational groups
390 based on phenotypic traits (67).

391 **Materials and Methods**

392 ***Data collection and DNA extraction, sequencing and processing***

393 In this study, we used a total of 173 samples collected from three types of lake systems described
394 previously (46), including: (a) 49 samples from Lake Michigan (2013 & 2015), (b) 62 samples
395 from Muskegon Lake (2013-2015; one of Lake Michigan's estuaries), and (c) 62 samples from
396 twelve inland lakes in Southeastern Michigan (2014-2015). For more details on sampling, please
397 see **Figure 1** and the *Field Sampling, DNA extraction, and DNA sequencing and processing*
398 sections within Chiang et al. (46). In all cases, water for microbial biomass samples were
399 collected and poured through a 210 μm and 20 μm bleach sterilized nitex mesh and sequential in-
400 line filtration was performed using 47 mm polycarbonate in-line filter holders (Pall Corporation,
401 Ann Arbor, MI, USA) and an E/S portable peristaltic pump with an easy-load L/S pump head
402 (Masterflex®, Cole Parmer Instrument Company, Vernon Hills, IL, USA) to filter first through a
403 3 μm isopore polycarbonate (TSTP, 47 mm diameter, Millipore, Billerica, MA, USA) and
404 second through a 0.22 μm Express Plus polyethersulfone membrane filters (47 mm diameter,
405 Millipore, MA, USA). The current study only utilized the 3 - 0.22 μm fraction for analyses.
406
407 DNA extractions and sequencing were performed as described in Chiang et al. (46). Fastq files
408 were submitted to NCBI sequence read archive under BioProject accession number
409 PRJNA414423 (inland lakes), PRJNA412983 (Lake Michigan), and PRJNA412984 (Muskegon
410 Lake). We analyzed the sequence data using MOTHUR V.1.38.0 (seed = 777; (Schloss et al.
411 2009) based on the MiSeq standard operating procedure and put together at the following link:

412 https://github.com/rprops/Mothur_oligo_batch. A combination of the Silva Database (release
413 123; (68)) and the freshwater TaxAss 16S rRNA database and pipeline (69) was used for
414 classification of operational taxonomic units (OTUs).
415
416 For the taxonomic analysis, each of the three lake datasets were analyzed separately and treated
417 with an OTU abundance threshold cutoff of at least 5 sequences in 10% of the samples in the
418 dataset (similar strategy to (70)). For comparison of taxonomic abundances across samples, each
419 of the three datasets were then rarefied to an even sequencing depth, which was 4,491 sequences
420 for Muskegon Lake samples, 5,724 sequences for the Lake Michigan samples, and 9,037
421 sequences for the inland lake samples. Next, the relative abundance at the OTU level was
422 calculated using the *transform_sample_counts()* function in the phyloseq R package (71) by
423 taking the count value and dividing it by the sequencing depth of the sample. For all other
424 taxonomic levels, the taxonomy was merged at certain taxonomic ranks using the *tax_glom()*
425 function in phyloseq (71) and the relative abundance was re-calculated.
426
427 ***Heterotrophic bacterial production measurements***
428 Muskegon Lake samples from 2014 and 2015 were processed for heterotrophic bacterial
429 production using the [^{3}H] leucine incorporation into bacterial protein in the dark method (72, 73).
430 At the end of the incubation with [^{3}H]-leucine, cold trichloroacetic acid-extracted samples were
431 filtered onto 0.2 µm filters that represented the leucine incorporation by the bacterial community.
432 Measured leucine incorporation during the incubation was converted to bacterial carbon
433 production rate using a standard theoretical conversion factor of 2.3 kg C per mole of leucine
434 (73).

435

436 ***Flow cytometry, measuring HNA and LNA***

437 In the field, a total of 1 mL of 20 μm filtered lake water were fixed with 5 μL of glutaraldehyde
438 (20% vol/vol stock), incubated for 10 minutes on the bench (covered with aluminum foil to
439 protect from light degradation), and then flash frozen in liquid nitrogen to later be stored in -
440 80°C freezer until later processing with a flow cytometer. Flow cytometry procedures followed
441 the protocol laid out in Props et al. (56), which also uses the samples presented in the current
442 study (Michigan and Muskegon samples). Samples were stained with SYBR Green I and
443 measured in triplicate. The lowest number of cells collected after denoising was 2342. HNA and
444 LNA groups were selected using the fixed gates introduced in Prest et al. (74) and plotted in
445 **Figure S10**. Cell counts were determined per HNA and LNA group and averaged over the three
446 replicates (giving rise to HNAcc and LNAcc). All cytometry data is available on the
447 FlowRepository database (75): inland lakes (ID:FR-FCM-ZY9J), Michigan and Muskegon
448 (ID:FR-FCM-ZYZN).

449

450 **Data analysis**

451 Processed data and analysis code for the following analyses can be found on the GitHub page for
452 this project at https://deneflab.github.io/HNA_LNA_productivity/.

453

454 ***HNA-LNA and HNA-Productivity Statistics and Regressions***

455 We tested the difference in absolute number of cells within HNA and LNA functional groups
456 across running analysis of variance with a post-hoc Tukey HSD test (*aov()* and *TukeyHSD();*
457 *stats* R package; (76). In addition, we tested the association of HNA and LNA to each other and

with productivity by running ordinary least squares regression with the *lm()* (*stats* R package; (76)).

Ranking correlation

Ranking correlation between variables was calculated using the Kendall rank correlation coefficient, using the *kendalltau()* function in Scipy (v1.0.0) or *cor()* in R (v3.2). The 'tau-b' implementation was used, which is able to deal with ties. Values range from -1 (strong disagreement) to 1 (strong agreement). The same statistic was used to assess the similarity between rankings of variable selection methods.

Centered-log ratio transform

First, following guidelines from Paliy & Shanker (77), Gloor et al. (3) and Quinn et al. (78), relative abundances of OTUs were transformed using a centered log-ratio (CLR) transformation before variable selection was applied. This means that the relative abundance $x_i$of a taxa was transformed according to the geometric mean of that sample, in which there are p taxa present:

$$x_i' = \log(x_i/(\prod_{j=1}^{p} x_j)^{1/p})$$

.

Zero values were replaced by $\delta = 1/p^2$. This was done using the scikit-bio package (www.scikit-bio.org, v0.4.1).

Lasso & stability selection

Scores were assigned to taxa based on an extension of the Lasso estimator, which is called *stability selection* (28). In the case of n samples, the Lasso estimator fits the following regression model:

$$\hat{\beta}^{\lambda} = \text{argmin}_{\beta \in \mathbb{R}^p} ||y - X\beta||_2^2 + \lambda \sum_{j=1}^{p} |\beta_j| \quad ,$$

in which X denotes the abundance table, y the target to predict, which either is HNA cell abundances (HNAcc) or LNA cell abundances (LNAcc), β the weight of each variable and λ is a regularization parameter which controls the complexity of the model and prevents overfitting. The Lasso performs an intrinsic form of variable selection, as the weights of certain variables will be put to zero.

Stability selection, when applied to the Lasso, is in essence an extension of the Lasso regression. It implements two types of randomizations to assign a score to the variables, and is therefore also called the *Randomized Lasso* (RL). The resulting RL score can be seen as the probability that a certain variable will be included in a Lasso regression model (*i.e.*, its weight will be non-zero when fitted). When performing stability selection, the Lasso is fitted to B different subsamples of the data of fraction $n/2$, denoted as X' and corresponding y'. A second randomization is added by introducing a weakness parameter α. In each model, the penalty λ changes to a randomly chosen value in the set $[\lambda, \lambda/\alpha]$, which means that a higher penalty will be assigned to a random subset of the total amount of variables. The Randomized Lasso therefore becomes:

$$\hat{\beta}^{\lambda} = \text{argmin}_{\beta \in \mathbb{R}^p} ||y' - X'\beta||_2^2 + \lambda \sum_{j=1}^{p} \frac{|\beta_j|}{w_j} \quad ,$$

where w_j is a random variable which is either α or 1. Next, the Randomized Lasso score (RL score) is determined by counting the number of times the weight of a variable was non-zero for

each of the B models and divided by B. Meinshausen and Bühlmann (28) show that, under stringent conditions, the number of falsely selected variables is controlled for the Randomized Lasso when the RL score is higher than 0.5. If λ is varied, one can determine the stability path, which is the relationship between π and λ for every variable. For our implementation, $B = 500$, $\alpha = 0.5$ and the highest score was selected in the stability path for which λ ranged from 10^{-3} until 10^{3}, logarithmically divided in 100 intervals. The *RandomizedLasso()* function from the scikit-learn machine learning library was used ((79), v0.19.1).

Random Forests & Boruta

The Boruta algorithm is a *wrapper* algorithm that makes use of Random Forests as a base classification or regression method in order to select all relevant variables in function of a response variable (29). Similar to stability selection, the method uses an additional form of randomness in order to perform variable selection. Random Forests are fitted to the data multiple times. To remove the correlation to the response variable, each variable gets per iteration a so-called *shadow variable*, which is a permuted copy of the original variable. Next, the Random Forest algorithm is run with the extended set of variables, after which variable importances are calculated for both original and shadow variables. The shadow variable that has the highest importance score is used as reference, and every variable with significantly lower importance, as determined by a Bonferroni corrected t-test, is removed. Likewise, variables containing an importance score that is significantly higher are included in the final list of selected variables. This procedure can be repeated until all original variables are either discarded or included in the final set; variables that remain get the label 'tentative' (i.e., after all repetitions it is still not possible to either select or discard a certain variable). We used the boruta_py package to

implement the Boruta algorithm (https://github.com/scikit-learn-contrib/boruta_py). Random Forests were implemented using *RandomForestRegressor()* function from scikit-learn (79), v0.19.1. Random Forests were run with 200 trees, the number of variables considered at every split of a decision tree was $p/3$ and the minimal number of samples per leaf was set to five. The latter were based on default values for Random Forests in a regression setting (80). The Boruta algorithm was run for 300 iterations, variables were selected or discarded at $P < .05$ after performing Bonferroni correction.

Recursive variable elimination

Scores of the Randomized Lasso were evaluated using a recursive variable elimination strategy (81). Variables were ranked according to the RL score. Next, the lowest-ranked variables were eliminated from the dataset, after which the Lasso was applied to predict HNAcc and LNAcc respectively. This process was repeated until only the highest-scored taxa remained. In this way, performance of the Randomized Lasso was assessed from a minimal-optimal evaluation perspective (82). In other words, the lowest amount of variables that resulted in the highest predictive performance was determined.

Performance evaluation

In order to account for the spatiotemporal structure of the data, a blocked cross-validation scheme was implemented (83). Samples were grouped according the site and year that they were collected. This results in 5, 10 and 16 distinctive groups for the Michigan, Muskegon and Inland lake systems respectively. Predictive models were optimized in function of the R^2 between predicted and true values of held-out groups using a leave-one-group-out cross-validation

546 scheme with the *LeaveOneGroupOut()* function. This results in a cross-validated R^2_{CV} value. For
547 the Lasso, λ was determined using the lassoCV() function, with setting eps=10^{-4} and
548 n_alphas=400. The Random Forest object was optimized using a grid search where max_features
549 was chosen in the interval $[1, \sqrt{p}, 2\sqrt{p}, ..., p]$ (all variables) or $[1, ..., p]$ (Boruta selected variables)
550 and min_samples_leaf in the interval $[1, ..., 5]$, using the *GridSearchCV()* function. The number
551 of decision trees (n_trees) was set to 200. All functions are part of scikit-learn ((79); v0.19.1)
552
553 ***Stability of the Randomized Lasso***
554 Similarity of RL scores between lake systems and functional groups was quantified using the
555 Pearson correlation. This was done using the *pearsonr()* function in Scipy (v1.0.0).
556
557 ***Patterns of HNA and LNA OTUs across ecosystems and phylogeny***
558 To visualize patterns of selected HNA and LNA OTUs across the three ecosystems, a heatmap
559 was created with the RL scores of each OTU from the Randomized Lasso regression that were
560 higher than specified threshold values. The heatmap was created with the *heatmap.2()* function
561 (*gplots* R package) using the euclidean distances of the RL scores and a complete linkage
562 hierarchical clustering algorithm (**Figure 4**).
563
564 ***Correlations between taxa and productivity measurements***
565 The Kendall ranking correlation coefficient or Kendall's tau-b between productivity
566 measurements and individual abundances were calculated on the phylum and OTU level using
567 the *kendalltau()* function from Scipy (v1.0.0). P-values were corrected using Benjamini-

Hochberg correction, reported as P_adj. This was done using the *multitest()* function from the Python module Statsmodels ((84); v0.5.0).

Phylogenetic tree construction and signal calculation

We calculated the best performing maximum likelihood tree using the GTR-CAT model (-gtr -fastest) model of nucleotide substitution with FastTree (version 2.1.9 No SSE3; (85)) and visualized using the interactive tree of life (iTOL) (86). Phylogenetic signal is a measure of the dependence among a species' trait values on their phylogenetic history (87). If the phylogenetic signal is very strong, taxa belonging to similar phylogenetic groups (*e.g.* a Phylum) will share the same trait (*i.e.* association with HNAcc or LNAcc). Alternatively, if the phylogenetic signal is weak, taxa within a similar phylogenetic group will have different traits. The phylogenetic signal was measured with both discrete (*i.e.* HNA, LNA, or both) and continuous traits (*i.e.* the RL score) using the newick tree from FastTree. For the most part, Pagel's lambda was used (88) to test for phylogenetic signal and was calculated with the fitDiscrete() function from the geiger R package (discrete trait; (89)) and the phylosig() function from the phytools R package (continuous trait; (90)). The lambda value varies between 0 and 1, with 1 indicating complete phylogenetic patterning and 0 representing no phylogenetic patterning, leading to a tree collapsing into a single polytomy. was then used to model phylogenetic signal using Pagel's lambda, Blomberg's K (phylosig() function from the phytools R package (90)), and Moran's I (abouheif.moran() function from the adephylo R package (91)).

Acknowledgements

PR was supported by Ghent University (BOFSTA2015000501) and MLS was supported by the National Science Foundation Graduate Research Fellowship Program (Grant No. DGE 1256260). Part of the computational resources (Stevin Supercomputer Infrastructure) and services used in this work were provided by the VSC (Flemish Supercomputer Center), funded by Ghent University, the Hercules Foundation and the Flemish Government department EWI. Flow cytometry analysis was supported through a Geconcerteerde Onderzoeksactie (GOA) from Ghent University (BOF15/GOA/006).

Author Contributions

MLS and PR co-wrote the paper with contributions from RP, BB, NB, WW, and VJD. MLS, RP, and BB generated the data. MLS, PR, and RP performed the data analysis. PR, MLS, RP, WW, and VJD designed the study.

References

1. Lennon JT, Jones SE. 2011. Microbial seed banks: the ecological and evolutionary implications of dormancy. Nature Reviews Microbiology 9:119–130.

2. Carini P, Marsden PJ, Leff JW, Morgan EE, Strickland MS, Fierer N. 2017. Relic DNA is abundant in soil and obscures estimates of soil microbial diversity. Nature Microbiology 2:16242.

3. Gloor GB, Macklaim JM, Pawlowsky-Glahn V, Egozcue JJ. 2017. Microbiome Datasets Are Compositional: And This Is Not Optional. Frontiers in Microbiology 8.

4. Knight R, Vrbanac A, Taylor BC, Aksenov A, Callewaert C, Debelius J, Gonzalez A, Kosciolek T, McCall L-I, McDonald D, Melnik AV, Morton JT, Navas J, Quinn RA, Sanders JG, Swafford AD, Thompson LR, Tripathi A, Xu ZZ, Zaneveld JR, Zhu Q, Caporaso JG, Dorrestein PC. 2018. Best practices for analysing microbiomes. Nature Reviews Microbiology 16:410–422.

5. Widder S, Allen RJ, Pfeiffer T, Curtis TP, Wiuf C, Sloan WT, Cordero OX, Brown SP, Momeni B, Shou W, Kettle H, Flint HJ, Haas AF, Laroche B, Kreft J-U, Rainey PB, Freilich S, Schuster S, Milferstedt K, van der Meer JR, Großkopf T, Huisman J, Free A, Picioreanu C, Quince C, Klapper I, Labarthe S, Smets BF, Wang H, Isaac Newton Institute Fellows, Soyer OS. 2016. Challenges in microbial ecology: building predictive understanding of community function and dynamics. The ISME Journal 10:2557–2568.

6. Gasol JM, Del Giorgio PA. 2000. Using flow cytometry for counting natural planktonic bacteria and understanding the structure of planktonic bacterial communities. Scientia Marina 64:197–224.

7. Vives-Rego J, Lebaron P, Nebe-von Caron G. 2000. Current and future applications of flow cytometry in aquatic microbiology. FEMS Microbiology Reviews 24:429–448.

8. Wang Y, Hammes F, De Roy K, Verstraete W, Boon N. 2010. Past, present and future applications of flow cytometry in aquatic microbiology. Trends in Biotechnology 28:416–424.

9. Gasol JM, Zweifel UL, Peters F, Fuhrman JA. 1999. Significance of Size and Nucleic Acid Content Heterogeneity as Measured by Flow Cytometry in Natural Planktonic Bacteria. Applied and Environmental Microbiology 65:4475–4483.

10. Lebaron P, Servais P, Agogue H, Courties C, Joux F. 2001. Does the high nucleic acid content of individual bacterial cells allow us to discriminate between active cells and inactive cells in aquatic systems? Applied and Environmental Microbiology 67:1775–1782.

11. Bouvier T, del Giorgio PA, Gasol JM. 2007. A comparative study of the cytometric characteristics of High and Low nucleic-acid bacterioplankton cells from different aquatic ecosystems. Environmental Microbiology 9:2050–2066.

12. Wang Y, Hammes F, Boon N, Chami M, Egli T. 2009. Isolation and characterization of low nucleic acid (LNA)-content bacteria. The ISME Journal 3:889–902.

13. Lebaron P, Servais P, Baudoux A, Bourrain M, Courties C, Parthuisot N. 2002. Variations of bacterial-specific activity with cell size and nucleic acid content assessed by flow cytometry. Aquatic Microbial Ecology 28:131–140.

14. Servais P, Casamayor E, Courties C, Catala P, Parthuisot N, Lebaron P. 2003. Activity and diversity of bacterial cells with high and low nucleic acid content. Aquatic Microbial Ecology 33:41–51.

15. Morán X, Bode A, Suárez L, Nogueira E. 2007. Assessing the relevance of nucleic acid content as an indicator of marine bacterial activity. Aquatic Microbial Ecology 46:141–152.

16. Servais P, Courties C, Lebaron P, Troussellier M. 1999. Coupling Bacterial Activity Measurements with Cell Sorting by Flow Cytometry. Microbial Ecology 38:180–189.

17. Bowman JS, Amaral-Zettler LA, J Rich J, M Luria C, Ducklow HW. 2017. Bacterial community segmentation facilitates the prediction of ecosystem function along the coast of the western Antarctic Peninsula. The ISME Journal 11:1460–1471.

18. Moràn XAG, Ducklow HW, Erickson M. 2011. Single-cell physiological structure and growth rates of heterotrophic bacteria in a temperate estuary (Waquoit Bay, Massachusetts). Limnology and Oceanography 56:37–48.

19. Read DS, Gweon HS, Bowes MJ, Newbold LK, Field D, Bailey MJ, Griffiths RI. 2015. Catchment-scale biogeography of riverine bacterioplankton. The ISME Journal 9:516–526.

20. Sherr EB, Sherr BF, Longnecker K. 2006. Distribution of bacterial abundance and cell-specific nucleic acid content in the Northeast Pacific Ocean. Deep Sea Research Part I: Oceanographic Research Papers 53:713–725.

21. García FC, Calleja ML, Al-Otaibi N, Røstad A, Morán XAG. 2018. Diel dynamics and coupling of heterotrophic prokaryotes and dissolved organic matter in epipelagic and mesopelagic waters of the central Red Sea. Environmental Microbiology 20:2990–3000.

22. Jochem FJ, Lavrentyev PJ, First MR. 2004. Growth and grazing rates of bacteria groups with different apparent DNA content in the Gulf of Mexico. Marine Biology 145:1213–1225.

23. Arnoldini M, Heck T, Blanco-Fernández A, Hammes F. 2013. Monitoring of Dynamic Microbiological Processes Using Real-Time Flow Cytometry. PLoS ONE 8:e80117.

24. Ramseier MK, von Gunten U, Freihofer P, Hammes F. 2011. Kinetics of membrane damage to high (HNA) and low (LNA) nucleic acid bacterial clusters in drinking water by ozone, chlorine, chlorine dioxide, monochloramine, ferrate(VI), and permanganate. Water Research 45:1490–1500.

25. Huete-Stauffer T, Morán X. 2012. Dynamics of heterotrophic bacteria in temperate coastal waters: similar net growth but different controls in low and high nucleic acid cells. Aquatic Microbial Ecology 67:211–223.

26. Morán XAG, Alonso-Sáez L, Nogueira E, Ducklow HW, González N, López-Urrutia Á, Díaz-Pérez L, Calvo-Díaz A, Arandia-Gorostidi N, Huete-Stauffer TM. 2015. More, smaller bacteria in response to ocean's warming? Proceedings of the Royal Society B: Biological Sciences 282:20150371.

679 27. Proctor CR, Besmer MD, Langenegger T, Beck K, Walser J-C, Ackermann M, Bürgmann
680 H, Hammes F. 2018. Phylogenetic clustering of small low nucleic acid-content bacteria
681 across diverse freshwater ecosystems. The ISME Journal 12:1344–1359.

682 28. Meinshausen N, Bühlmann P. 2010. Stability selection: Stability Selection. Journal of the
683 Royal Statistical Society: Series B (Statistical Methodology) 72:417–473.

684 29. Kursa MB, Rudnicki WR. 2010. Feature Selection with the **Boruta** Package. Journal of
685 Statistical Software 36.

686 30. Li H. 2015. Microbiome, Metagenomics, and High-Dimensional Compositional Data
687 Analysis. Annual Review of Statistics and Its Application 2:73–94.

688 31. Strobl C, Boulesteix A-L, Kneib T, Augustin T, Zeileis A. 2008. Conditional variable
689 importance for random forests. BMC Bioinformatics 9.

690 32. Biddanda B. 2017. Global Significance of the Changing Freshwater Carbon Cycle. Eos
691 98:1–5.

692 33. Salcher MM, Posch T, Pernthaler J. 2013. *In situ* substrate preferences of abundant
693 bacterioplankton populations in a prealpine freshwater lake. The ISME Journal 7:896–907.

694 34. Schubert AM, Rogers MAM, Ring C, Mogle J, Petrosino JP, Young VB, Aronoff DM,
695 Schloss PD. 2014. Microbiome Data Distinguish Patients with *Clostridium difficile*
696 Infection and Non-*C. difficile*-Associated Diarrhea from Healthy Controls. mBio 5.

697 35. Baxter NT, Zackular JP, Chen GY, Schloss PD. 2014. Structure of the gut microbiome
698 following colonization with human feces determines colonic tumor burden. Microbiome
699 2:20.

700 36. Herren CM, McMahon KD. 2018. Keystone taxa predict compositional change in microbial
701 communities: Keystone microbes predict community turnover. Environmental
702 Microbiology 20:2207–2217.

703 37. Lin W, Shi P, Feng R, Li H. 2014. Variable selection in regression with compositional
704 covariates. Biometrika 101:785–797.

705 38. Zaura E, Brandt BW, Prodan A, Teixeira de Mattos MJ, Imangaliyev S, Kool J, Buijs MJ,
706 Jagers FL, Hennequin-Hoenderdos NL, Slot DE, Nicu EA, Lagerweij MD, Janus MM,
707 Fernandez-Gutierrez MM, Levin E, Krom BP, Brand HS, Veerman EC, Kleerebezem M,
708 Loos BG, van der Weijden GA, Crielaard W, Keijser BJ. 2017. On the ecosystemic
709 network of saliva in healthy young adults. The ISME Journal 11:1218–1231.

710 39. Chen J, Chia N, Kalari KR, Yao JZ, Novotna M, Soldan MMP, Luckey DH, Marietta EV,
711 Jeraldo PR, Chen X, Weinshenker BG, Rodriguez M, Kantarci OH, Nelson H, Murray JA,
712 Mangalam AK. 2016. Multiple sclerosis patients have a distinct gut microbiota compared to
713 healthy controls. Scientific Reports 6:28484.

714 40. Ma J, Prince AL, Bader D, Hu M, Ganu R, Baquero K, Blundell P, Alan Harris R, Frias
715 AE, Grove KL, Aagaard KM. 2014. High-fat maternal diet during pregnancy persistently
716 alters the offspring microbiome in a primate model. Nature Communications 5:3889.

41. Degenhardt F, Seifert S, Szymczak S. 2017. Evaluation of variable selection methods for random forests and omics data sets. Briefings in Bioinformatics.

42. McCarthy A, Chiang E, Schmidt ML, Denef VJ. 2015. RNA Preservation Agents and Nucleic Acid Extraction Method Bias Perceived Bacterial Community Composition. PLOS ONE 10:e0121659.

43. Louca S, Doebeli M, Parfrey LW. 2018. Correcting for 16S rRNA gene copy numbers in microbiome surveys remains an unsolved problem. Microbiome 6:41.

44. Van der Gucht K, Cottenie K, Muylaert K, Vloemans N, Cousin S, Declerck S, Jeppesen E, Conde-Porcuna J-M, Schwenk K, Zwart G, Degans H, Vyverman W, De Meester L. 2007. The power of species sorting: Local factors drive bacterial community composition over a wide range of spatial scales. Proceedings of the National Academy of Sciences 104:20404–20409.

45. Adams HE, Crump BC, Kling GW. 2014. Metacommunity dynamics of bacteria in an arctic lake: the impact of species sorting and mass effects on bacterial production and biogeography. Frontiers in Microbiology 5.

46. Chiang E, Schmidt ML, Berry MA, Biddanda BA, Burtner A, Johengen TH, Palladino D, Denef VJ. 2018. Verrucomicrobia are prevalent in north-temperate freshwater lakes and display class-level preferences between lake habitats. PLOS ONE 13:e0195112.

47. Aanderud ZT, Vert JC, Lennon JT, Magnusson TW, Breakwell DP, Harker AR. 2016. Bacterial Dormancy Is More Prevalent in Freshwater than Hypersaline Lakes. Frontiers in Microbiology 7.

48. Jones SE, Lennon JT, Karl D. 2010. Dormancy contributes to the maintenance of microbial diversity. Proceedings of the National Academy of Sciences of the United States of America 107:5881–5886.

49. Zimmermann R, Iturriaga R, Becker-Birck J. 1978. Simultaneous Determination of the Total Number of Aquatic Bacteria and the Number Thereof Involved in Respiration. Applied and Environmental Microbiology 36:926–935.

50. Corno G, Jürgens K. 2006. Direct and Indirect Effects of Protist Predation on Population Size Structure of a Bacterial Strain with High Phenotypic Plasticity. Applied and Environmental Microbiology 72:78–86.

51. Coleman ML, Sullivan MB, Martiny AC, Steglich C, Barry K, DeLong EF, Chisholm SW. 2006. Genomic islands and the ecology and evolution of *Prochlorococcus*. Science 311:1768–1770.

52. Hunt DE, David LA, Gevers D, Preheim SP, Alm EJ, Polz MF. 2008. Resource Partitioning and Sympatric Differentiation Among Closely Related Bacterioplankton. Science 320:1081–1085.

53. Denef VJ, Kalnejais LH, Mueller RS, Wilmes P, Baker BJ, Thomas BC, VerBerkmoes NC, Hettich RL, Banfield JF. 2010. Proteogenomic basis for ecological divergence of closely related bacteria in natural acidophilic microbial communities. Proceedings of the National Academy of Sciences 107:2383–2390.

757 54. Shapiro BJ, Polz MF. 2014. Ordering microbial diversity into ecologically and genetically
758 cohesive units. Trends in Microbiology 22:235–247.

759 55. Vila-Costa M, Gasol JM, Sharma S, Moran MA. 2012. Community analysis of high- and
760 low-nucleic acid-containing bacteria in NW Mediterranean coastal waters using 16S rDNA
761 pyrosequencing: Bacterial composition of different cytometric populations in
762 Mediterranean waters. Environmental Microbiology 14:1390–1402.

763 56. Props R, Schmidt ML, Heyse J, Vanderploeg HA, Boon N, Denef VJ. 2018. Flow
764 cytometric monitoring of bacterioplankton phenotypic diversity predicts high population-
765 specific feeding rates by invasive dreissenid mussels: Phenotypic tracking of
766 bacterioplankton. Environmental Microbiology 20:521–534.

767 57. Props R, Kerckhof F-M, Rubbens P, De Vrieze J, Hernandez Sanabria E, Waegeman W,
768 Monsieurs P, Hammes F, Boon N. 2017. Absolute quantification of microbial taxon
769 abundances. The ISME Journal 11:584–587.

770 58. Amalfitano S, Fazi S, Ejarque E, Freixa A, Romaní AM, Butturini A. 2018. Deconvolution
771 model to resolve cytometric microbial community patterns in flowing waters:
772 Deconvolving Cytometric Microbial Subgroups. Cytometry Part A 93:194–200.

773 59. Song Y, Wang Y, Mao G, Gao G, Wang Y. 2019. Impact of planktonic low nucleic acid-
774 content bacteria to bacterial community structure and associated ecological functions in a
775 shallow lake. Science of The Total Environment 658:868–878.

776 60. Schattenhofer M, Wulf J, Kostadinov I, Glöckner FO, Zubkov MV, Fuchs BM. 2011.
777 Phylogenetic characterisation of picoplanktonic populations with high and low nucleic acid
778 content in the North Atlantic Ocean. Systematic and Applied Microbiology 34:470–475.

779 61. Newton RJ, Jones SE, Eiler A, McMahon KD, Bertilsson S. 2011. A Guide to the Natural
780 History of Freshwater Lake Bacteria. Microbiology and Molecular Biology Reviews 75:14–
781 49.

782 62. Woodhouse JN, Kinsela AS, Collins RN, Bowling LC, Honeyman GL, Holliday JK, Neilan
783 BA. 2016. Microbial communities reflect temporal changes in cyanobacterial composition
784 in a shallow ephemeral freshwater lake. The ISME Journal 10:1337–1351.

785 63. Tada Y, Suzuki K. 2016. Changes in the community structure of free-living heterotrophic
786 bacteria in the open tropical Pacific Ocean in response to microalgal lysate-derived
787 dissolved organic matter. FEMS Microbiology Ecology 92:fiw099.

788 64. Vandeputte D, Kathagen G, D'hoe K, Vieira-Silva S, Valles-Colomer M, Sabino J, Wang J,
789 Tito RY, De Commer L, Darzi Y, Vermeire S, Falony G, Raes J. 2017. Quantitative
790 microbiome profiling links gut community variation to microbial load. Nature.

791 65. Frossard A, Hammes F, Gessner MO. 2016. Flow Cytometric Assessment of Bacterial
792 Abundance in Soils, Sediments and Sludge. Frontiers in Microbiology 7.

793 66. Foladori P, Bruni L, Tamburini S, Ziglio G. 2010. Direct quantification of bacterial biomass
794 in influent, effluent and activated sludge of wastewater treatment plants by using flow
795 cytometry. Water Research 44:3807–3818.

67. Couradeau E, Sasse J, Goudeau D, Nath N, Hazen TC, Bowen BP, Malmstrom RR, Northen TR. 2018. Study of Oak Ridge soils using BONCAT-FACS-Seq reveals that a large fraction of the soil microbiome is active. bioRxiv.

68. Quast C, Pruesse E, Yilmaz P, Gerken J, Schweer T, Yarza P, Peplies J, Glöckner FO. 2012. The SILVA ribosomal RNA gene database project: improved data processing and web-based tools. Nucleic Acids Research 41:D590–D596.

69. Rohwer RR, Hamilton JJ, Newton RJ, McMahon KD. 2018. TaxAss: Leveraging a Custom Freshwater Database Achieves Fine-Scale Taxonomic Resolution. mSphere 3:e00327-18.

70. Weiss S, Van Treuren W, Lozupone C, Faust K, Friedman J, Deng Y, Xia LC, Xu ZZ, Ursell L, Alm EJ, Birmingham A, Cram JA, Fuhrman JA, Raes J, Sun F, Zhou J, Knight R. 2016. Correlation detection strategies in microbial data sets vary widely in sensitivity and precision. The ISME Journal 10:1669–1681.

71. McMurdie PJ, Holmes S. 2013. phyloseq: An R Package for Reproducible Interactive Analysis and Graphics of Microbiome Census Data. PLoS ONE 8:e61217.

72. Kirchman D, K'Nees E, Hodson R. 1985. Leucine Incorporation and Its Potential as a Measure of Protein Synthesis by Bacteria in Natural Aquatic Systemst. Applied and Environmental Microbiology 49:9.

73. Simon M, Azam F. 1989. Protein content and protein synthesis rates of planktonic marine bacteria. Marine Ecology Progress Series 51:201–213.

74. Prest EI, Hammes F, Kötzsch S, van Loosdrecht MCM, Vrouwenvelder JS. 2013. Monitoring microbiological changes in drinking water systems using a fast and reproducible flow cytometric method. Water Research 47:7131–7142.

75. Spidlen J, Breuer K, Rosenberg C, Kotecha N, Brinkman RR. 2012. FlowRepository: A resource of annotated flow cytometry datasets associated with peer-reviewed publications. Cytometry Part A 81A:727–731.

76. R Core Team. 2018. R: A Language and Environment for Statistical Computing. R Foundation for Statistical Computing, Vienna, Austria.

77. Paliy O, Shankar V. 2016. Application of multivariate statistical techniques in microbial ecology. Molecular Ecology 25:1032–1057.

78. Quinn TP, Erb I, Richardson MF, Crowley TM. 2018. Understanding sequencing data as compositions: an outlook and review. Bioinformatics 34:2870–2878.

79. Pedregosa F, Varoquaux G, Gramfort A, Michel V, Thirion B, Grisel O, Blondel M, Prettenhofer P, Weiss R, Dubourg V, Vanderplas J, Passos A, Cournapeau D. Scikit-learn: Machine Learning in Python. MACHINE LEARNING IN PYTHON 6.

80. Probst P, Wright M, Boulesteix A-L. 2018. Hyperparameters and Tuning Strategies for Random Forest.

81. Guyon I, Weston J, Barnhill S. 2002. Gene Selection for Cancer Classification using Support Vector Machines. Machine Learning 46:389–422.

834 82. Nilsson R, Bjorkegren J, Tegner J. Consistent Feature Selection for Pattern Recognition in
835 Polynomial Time 24.

836 83. Roberts DR, Bahn V, Ciuti S, Boyce MS, Elith J, Guillera-Arroita G, Hauenstein S, Lahoz-
837 Monfort JJ, Schröder B, Thuiller W, Warton DI, Wintle BA, Hartig F, Dormann CF. 2017.
838 Cross-validation strategies for data with temporal, spatial, hierarchical, or phylogenetic
839 structure. Ecography 40:913–929.

840 84. Seabold S, Perktold J. 2010. Statsmodels: Econometric and Statistical Modeling with
841 Python. Proceedings of the 9th Python in Science Conference (SciPy 2010) 57–61.

842 85. Price MN, Dehal PS, Arkin AP. 2010. FastTree 2 – Approximately Maximum-Likelihood
843 Trees for Large Alignments. PLoS ONE 5:e9490.

844 86. Letunic I, Bork P. 2016. Interactive tree of life (iTOL) v3: an online tool for the display and
845 annotation of phylogenetic and other trees. Nucleic Acids Research 44:W242–W245.

846 87. Revell LJ, Harmon LJ, Collar DC. 2008. Phylogenetic Signal, Evolutionary Process, and
847 Rate. Systematic Biology 57:591–601.

848 88. Pagel M. 1999. Inferring the historical patterns of biological evolution. Nature 401:877–
849 884.

850 89. Harmon LJ, Weir JT, Brock CD, Glor RE, Challenger W. 2008. GEIGER: investigating
851 evolutionary radiations. Bioinformatics 24:129–131.

852 90. Revell LJ. 2012. phytools: an R package for phylogenetic comparative biology (and other
853 things). Methods in Ecology and Evolution 3:217–223.

854 91. Jombart T, Balloux F, Dray S. 2010. adephylo: new tools for investigating the phylogenetic
855 signal in biological traits. Bioinformatics 26:1907–1909.

856

Figure 1: (A) Correlation between HNA cell counts and LNA cell counts across the three freshwater lake ecosystems. **(B-D)** Muskegon Lake bacterial heterotrophic production and its correlation with **(B)** HNA cell counts (HNAcc), **(C)** LNA cell counts, (LNAcc) and **(D)** total cell counts. The grey area in plots A, B, and D represents the 95% confidence intervals.

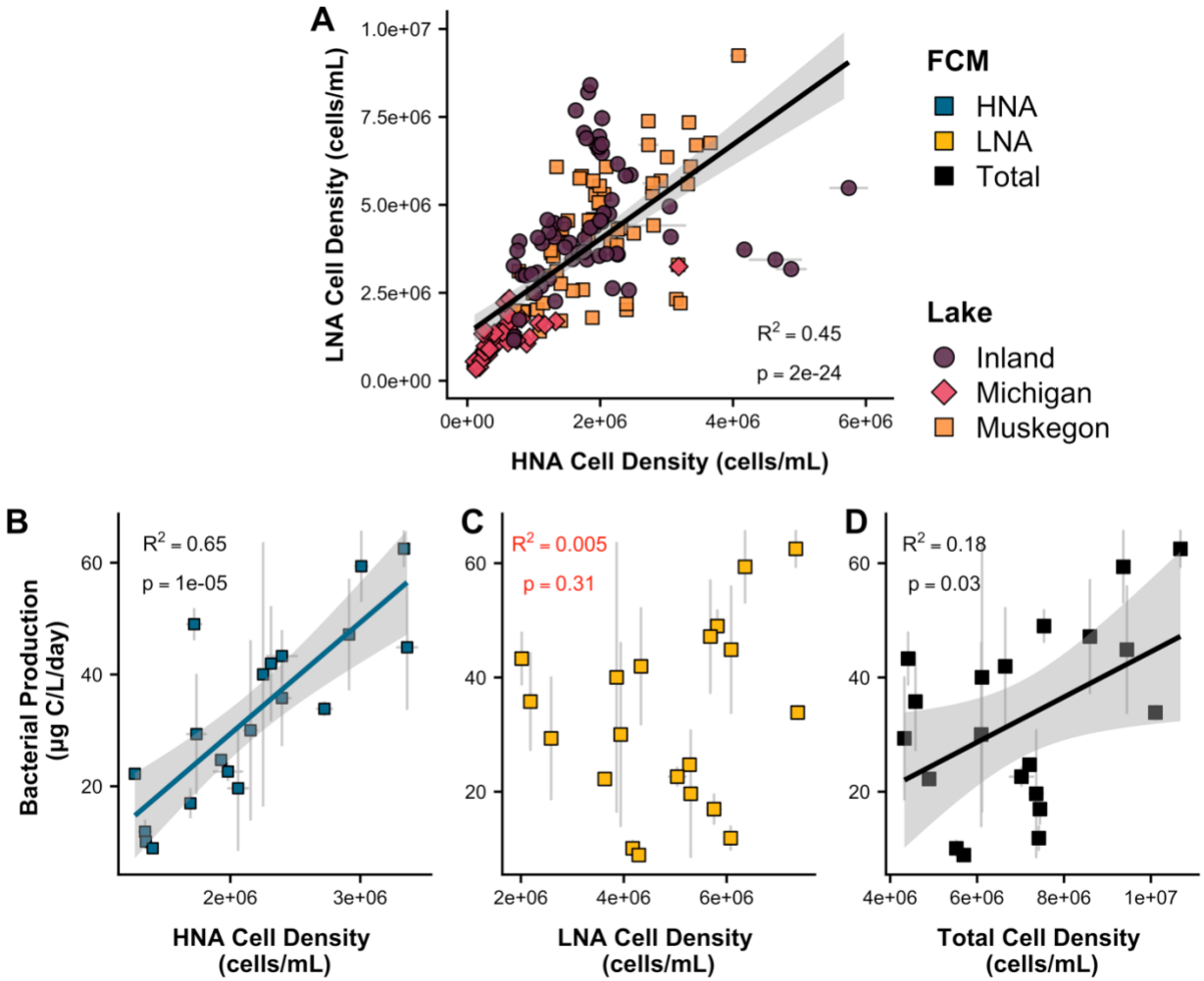

863 **Figure 2:** R^2_{CV} in function of the number of OTUs, which were iteratively removed based on the
864 RL score and evaluated using the Lasso at every step. The solid (HNA) and dashed (LNA)
865 vertical lines corresponds to the threshold (i.e., number of OTUs) which resulted in a maximal
866 R^2_{CV}. **(A)** Inland system ($R^2_{CV,max} = 0.92$), HNAcc; **(B)** Lake Michigan ($R^2_{CV,max} = 0.53$),
867 HNAcc; **(C)** Muskegon lake, HNAcc ($R^2_{CV,max} = 0.85$); **(D)** Inland system, LNAcc ($R^2_{CV,max} =$
868 0.87); **(E)** Lake Michigan, LNAcc ($R^2_{CV,max} = 0.79$; **(F)** Muskegon lake, LNAcc ($R^2_{CV,max} =$
869 0.91).

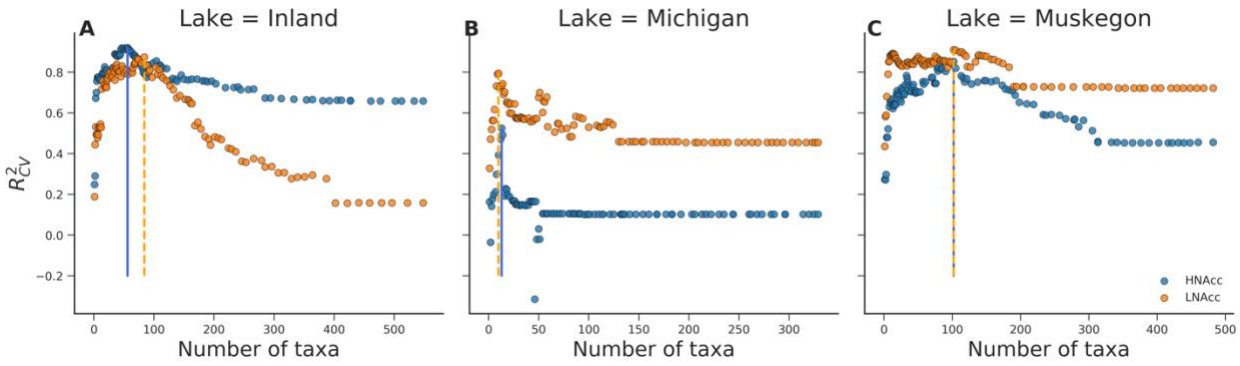

870

Figure 3: Evaluation of HNA cell counts (HNAcc) and LNA cell counts (LNAcc) predictions using the Lasso at all taxonomic levels for the Muskegon lake system, expressed in terms of R^2_{CV}, using different subsets of taxonomic variables. Subsets were determined by iteratively eliminating the lowest-ranked taxonomic variables based on the RL score.

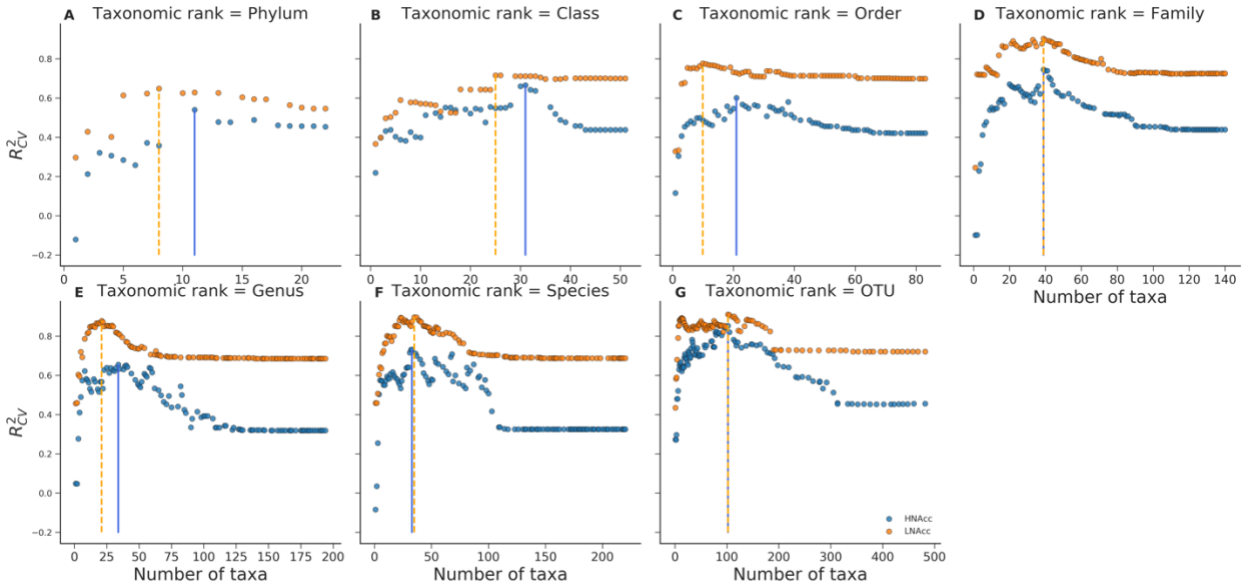

876 **Figure 4:** Hierarchical clustering of the RL score for the top 10 selected OTUs within each lake
877 system and FCM functional groups with the selected OTU (rows) across HNA and LNA groups
878 within the three lake systems (columns).

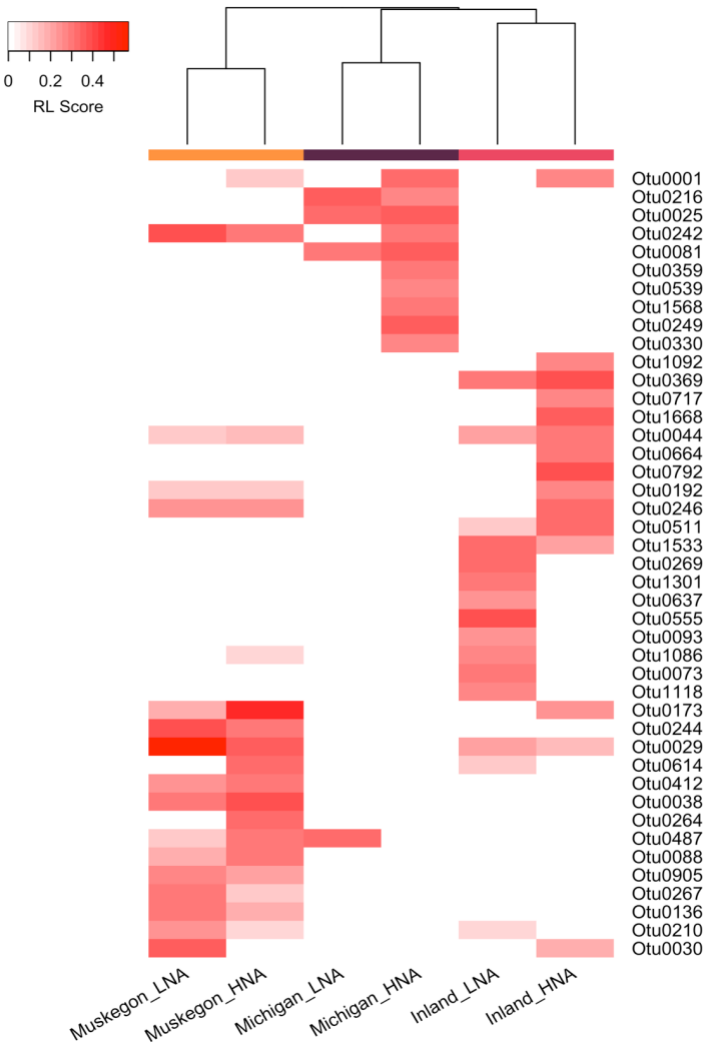

879

880 **Figure 5:** Phylogenetic tree with all HNA and LNA selected OTUs from each of the three lake
881 systems with their (*starting from the inside working to the outside*) (i) phylum level taxonomic
882 classification, (ii) HNA RL scores (*i.e.* HNA-Score), (iii) LNA RL scores (*i.e.* LNA-Score), and
883 (iv) and discrete association with HNA, LNA or both groups based on the RL score threshold
884 values (*i.e.* FCM-Group). Any OTU absent from a FCM group is white. The tree was rooted
885 using OTU1552.

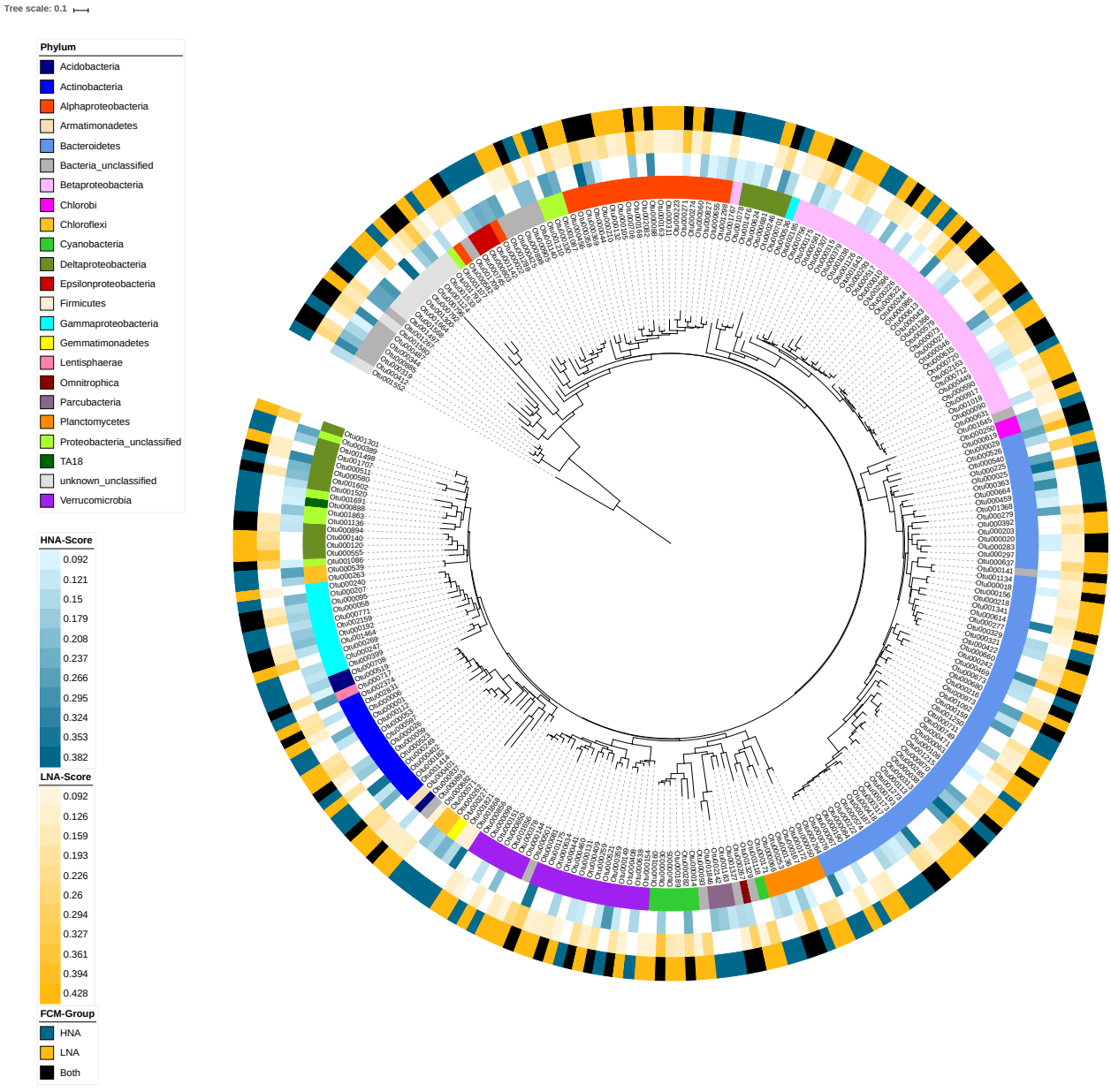

886

887 **Figure 6:** Correlation (Kendall's tau-b) between the relative abundances of the top three OTUs
888 selected by the RL and the densities in the cytometric fingerprint. The fluorescence threshold
889 used to manually define HNA and LNA populations is indicated by the dotted line.

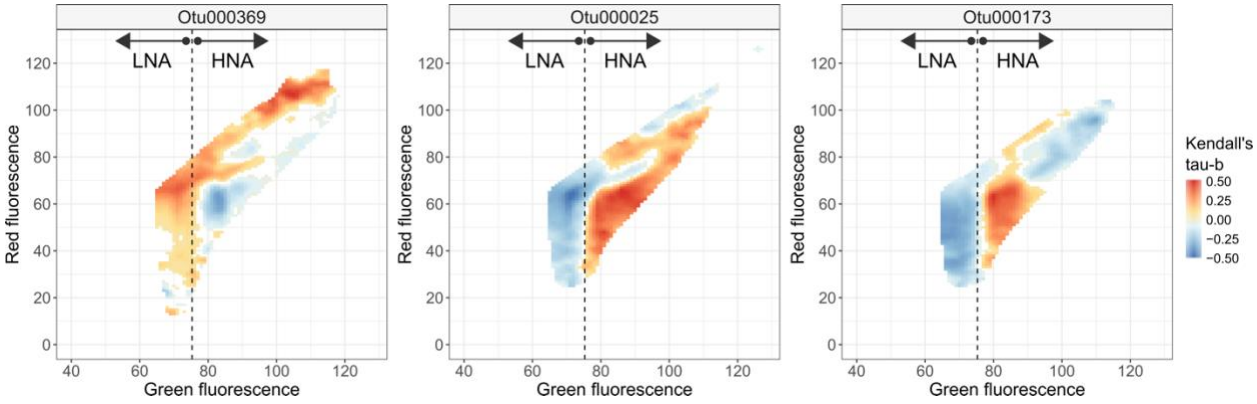

890

Table 1: Top scored OTUs according to the RL per functional population and lake ecosystem. Selection according to the Boruta algorithm is given in addition to the RL score. Descriptive statistics by means of the Kendall rank correlation coefficient have been added with level of significance in function of the HNA/LNA population.

Lake system	Functional group	OTU	RL score	Boruta selected	Kendall tau (HNA)	P-value (HNA)	Kendall tau (LNA)	P-value (LNA)	Phylum	Class	Order	Family	Genus (species)
Inland	HNA	OTU 369	0.382	yes	-0.43	<0.001	-0.28	0.0012	Proteobacteria	Alphaproteobacteria	Rhodospirrlalleles	alfVIII	alfVIII_ unclassified
	LNA	OTU 555	0.384	no	0.089	N.S.	0.22	0.011	Proteobacteria	Deltaproteobacteria	Bdellovibrionales	Bdellovibrionacea	OM27_clade
Michigan	HNA	OTU 025	0.362	yes	0.46	<0.001	0.41	<0.001	Bacteroidetes	Cytophagia	Cytophagales	bacIII	bacIII-A
	LNA	OTU 168	0.428	yes	0.26	0.0092	0.4	<0.001	Proteobacteria	Alphaproteobacteria	Rhizobiales	alfVII	alfVII_unclassified
Muskegon	HNA	OTU 173	0.462	yes	0.5	<0.001	0.2	0.019	Bacteroidetes	Flavobacteriia	Flavobacteriales	bacII	bacII-A
	LNA	OTU 029	0.568	no	0.26	0.0029	0.49	<0.001	Bacteroidetes	Cytophagia	Cytophagales	bacIII	bacIII-B (Algor)